In Situ Studies of Phase Transformation and Residual Stresses in LTT Alloys During Welding Using Synchrotron Radiation

Arne Kromm, Thomas Kannengiesser and Jens Gibmeier

Abstract Novel martensitic filler materials with specially adjusted martensite start temperatures (M_s) can counteract the cooling specific shrinkage due to expansion effects of the weld metal associated with phase transformations. That can be exploited to create compressive residual stresses in the weld and adjacent areas, i.e. beneficial for increasing the fatigue strength. The M_s temperature is shifted via the chemical composition, mainly by the alloying elements nickel and chromium, resulting as well in different retained austenite contents. Comparative investigations were made using a Low Transformation Temperature (LTT) alloy and a conventional high strength steel. The resulting phase transformation temperatures were—for the first time—detected using high energy synchrotron diffraction. Compared to angle dispersive diffraction, energy dispersive diffraction offers the possibility to measure residual stresses of the martensite and austenite phase parallel fast in one experiment. Furthermore, the high energy allows for obtaining information from the material volume by measuring in transmission geometry. For that purpose a special welding setup was designed applicable at different beam-lines and diffraction setups, allowing for diffraction experiments under realistic welding conditions. In particular the setup gives the possibility to observe and correlate localized phase transformations and thermo-mechanical stress/strain evolution during and after welding specific, rapid heat treatments. Additionally, due to local melting, solidification processes can be investigated. First results, presented here, show the correlation of local residual stress distributions affected by lowered transformation temperature.

A. Kromm (✉) and T. Kannengiesser
BAM Federal Institute for Materials Research and Testing, Unter den Eichen 87, 12205, Berlin, Germany
e-mail: arne.kromm@bam.de

J. Gibmeier
Karlsruhe Institute of Technology (KIT), Kaiserstr. 12, 76131, Karlsruhe, Germany

T. Kannengiesser et al. (eds.), *In-situ Studies with Photons, Neutrons and Electrons Scattering*, DOI: 10.1007/978-3-642-14794-4_2,

1 Introduction

When welding ferritic steels specific residual stresses due to inhomogeneous temperature distribution and phase transformations occur in the vicinity of the weld. For alloys with γ–α' phase transformations at relatively low temperatures (so-called (Low transformation Temperature (LTT) materials) their yield limit is already high enough, that phase transformations can affect the residual stress formation substantially. The impact of phase transformations at low temperatures on the residual stress formation can in principle be explained as follows. Since the thermal expansion coefficient of austenite is higher than that of ferrite, the volume expansion by the phase transformation is larger at low temperatures. In addition—following Bhadeshia (2004)—it can be stated that during cooling a high shrinkage compensation of the face-centered cubic lattice and thus lower stresses are present, caused by the lower yield point of austenite compared to ferrite. In contrast, smaller shrinkage compensation is present in the body-centered cubic lattice of ferrite due to the higher yield point, which leads to comparatively high stress gradients. Using lowered martensite transformation temperatures ($M_{s/f}$) it should finally be possible to avoid crack-critical tensile residual stresses in the weld and adjacent areas or even to produce compressive residual stresses already during the welding process. Such materials can essentially contribute to the improvement of the cold cracking resistance and fatigue strength of high strength steel welds (Ohta et al. 1999; Wang et al. 2002; Eckerlid et al. 2003; Dai et al. 2008; Kannengiesser et al. 2008).

Recent investigations dealt with the influence of the chemical composition of various LTT alloys on microstructure, transformation temperature and the resulting residual stresses. The local and temporary very rapid temperature gradients during welding make these investigations complex and hardly accessible by in situ observation. Diffraction methods represent an appropriate method to observe phase transformations in in situ during a certain loading or temperature cycle accompanied by the essential advantage of simultaneous strain measurement. Therefore diffraction methods are more and more used to analyze material behavior during welding. Apart from short time-metallurgy—i.e. the identification of the primary solidification mode—also phase transformations and their kinetics can be observed. However, previous investigations were limited to material ranges near the surface due to their measuring setup or limited beam characteristics. First in situ diffraction analyses of the transformation behavior during welding were conducted by Elmer et al. (2000), Babu et al. (2002) and Terasaki et al. (2006). They used low-energy, monochromatic synchrotron radiation with photon energies within a range of 7 to 12 keV (angle dispersive diffraction). In the present work for the first time high energy, polychromatic synchrotron radiation could be used for the characterization of the material behavior during welding. High energy synchrotron radiation up to 150 keV permits spatial and time resolved analyses in discrete material volumes of higher information depths. Furthermore the employment of energy dispersive methods allows for comfortable observation of

phase kinetics using complete diffraction patterns. Additionally, the resulting residual stresses of all contributing crystalline phases can be reliably determined.

2 Material

Following the concept presented by Ohta et al. (1999) of high-strength LTT welding fillers, own alloy concepts were developed in order to investigate the residual stress formation depending on varying M_s temperatures and material properties (Kromm et al. 2009). The pure LTT alloy (see Table 1) exemplary used in this investigation shows a M_s temperature of 39°C. This temperature was determined by single sensor—differential thermal analysis (SS-DTA) after Alexandrov and Lippold (2004). All weld metal specimens were austenitized at 850°C and subsequently quenched in oil down to ambient temperature. An exponential function served as reference curve. The M_s temperature was confirmed by means of time resolved energy dispersive synchrotron diffraction (Kromm and Kannengiesser 2009).

The resulting microstructure after welding consists of martensite and retained austenite like shown in Fig. 1. The primary solidification is austenitic and cellular. The cell cores are predominantly martensitic. The austenite is present network-like within inter-cellular areas, where due to segregation higher chrome and nickel contents are present. Localized EBSD measurements presented in Fig. 2 prove that austenite is to be found primarily within the inter-cellular areas. Additional

Table 1 Chemical composition (wt%) and transformation temperature of the applied LTT alloy

C	Ni	Cr	Mn	Si	Fe	M_s
0.04	12	10	0.7	0.4	Balance	39°C

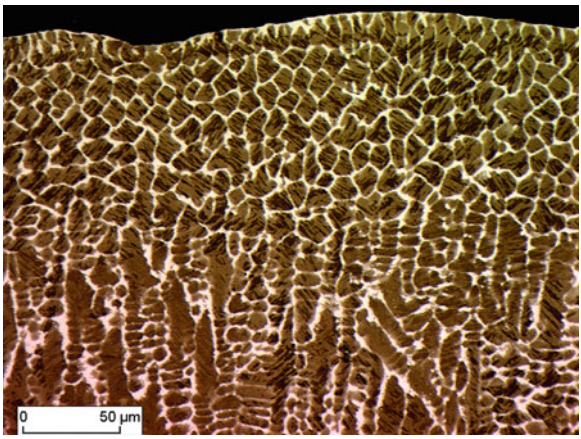

Fig. 1 Weld microstructure consisting of martensite (*dark colored areas* = lower Cr/Ni content) and retained austenite (*light colored areas* = higher Cr/Ni content)—etchant: Lichtenegger and Bloech

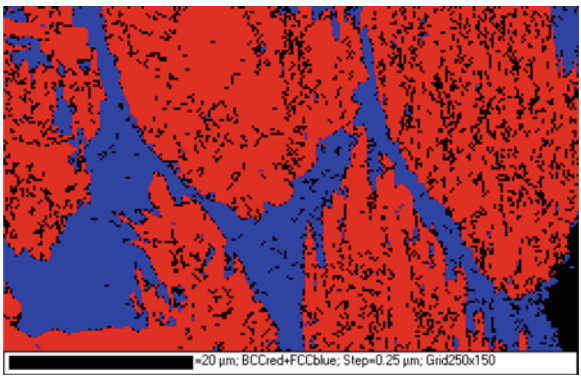

Fig. 2 EBSD image showing martensitic cells (*light grey*), austenite network (*dark grey*) and not classified areas (*black*)

microanalysis on welds specimens have confirmed that the segregation profile of chromium and nickel is similar, showing lower contents of both elements in martensite areas.

The fine-grained, high-strength, structural steel S690Q was used as base material as well for comparative bead-on-plate welding investigations (Table 2). The transformation temperature of this type of steel is cooling rate dependent and typically situated between 400 and 500°C. The microstructure after welding predominantly consists of bainite and some percent of ferrite or martensite.

3 Experimental

Welding and Diffraction Setup

In situ diffraction during welding were conducted with high energy, polychromatic synchrotron radiation (white beam) with photon energies between 20 and 150 keV, available at the beam-line EDDI of the Helmholtz association at the BESSY II storage ring in Berlin (Genzel et al. 2007). Energy dispersive (ED) diffraction experiments were carried out, in order to obtain a multitude of diffraction lines of all crystalline phases of the material simultaneously within one measurement. ED diffraction allows for evaluation of the lattice spacing $d(hkl)$ is a function of the corresponding Energy $E(hkl)$ measured under a fixed diffraction angle θ, see (Genzel et al. 2007) for details. In addition the beam-line setup permits for subsequent determination of the phase-specific residual stresses using the $\sin^2 \psi$ technique (Macherauch and Müller 1961; Spiess et al. 2009). A special experimental setup was

Table 2 Chemical composition of S690Q (wt%)

C	Si	Mn	P	S	Cr	Ni	Mo	Nb	V	B
0.116	0.402	1.52	0.017	<0.001	0.498	0.481	0.111	<0.005	0.054	0.0005

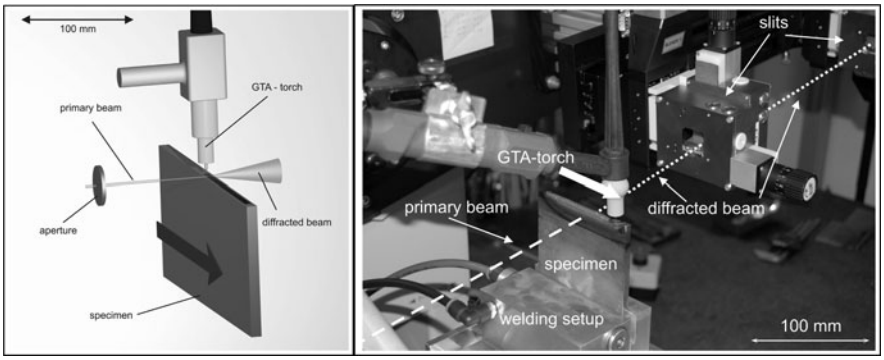

Fig. 3 Experimental setup schematically and arrangement at the beam-line including beam path

developed, what allows for time as well as spatial resolved diffraction experiments during real welding. The high energy synchrotron radiation enables in situ diffraction analyses in transmission geometry and permits access to the specimen volume. The local gauge volume is determined by primary and secondary beam apertures (slit system). The experimental setup is shown schematically in Fig. 3.

In situ ED diffraction analyses was conducted during gas tungsten arc (GTA) welding (re-melting). The specimens were prepared by pre-welding the LTT alloy in four layers on the upper edge of a plate made of S690Q high-strength steel. Subsequently, the weld was machined to ensure dimensions of 100 mm × 100 mm × 6 mm (length × width × thickness). Figure 4 shows the generated measuring volume schematically in the sample cross section. For purposes of comparison similar specimens of the material S690Q were prepared. In the present case the experiments were performed as time resolved analyses. Thereby, the beam hits the specimen at a fixed position while the torch is moved along the upper edge of specimen.

Five locations in the specimen were chosen for in situ analysis. The measuring range is shown in Fig. 5. The weld was investigated stepwise starting 1 mm below the surface and ending up 5 mm below the surface. Table 3 shows the measuring and evaluation parameters used.

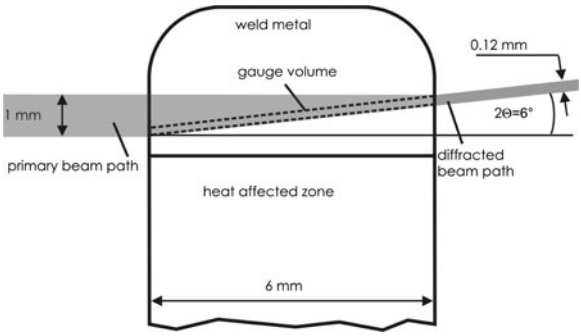

Fig. 4 Beam path and gauge volume generated in the specimen cross-section

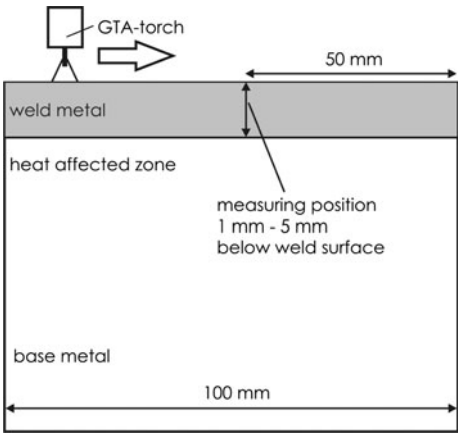

Fig. 5 Measuring range on the specimen

Table 3 Measuring and evaluation parameters

Primary beam cross-section	1×1 mm^2
Secondary aperture	Double slit system (equatorial $\times$ axial) 0.12 mm $\times$ 5 mm
Diffraction angle	$2\Theta = 6°$
Measuring mode	Transmission
Measuring time	7 s/spectrum
Evaluated diffraction lines	Ferrite/martensite: 110, 200, 211; austenite: 111, 220, 311

Essential for characterization of the phase transformations and associated residual stresses is the knowledge of the content of martensite and austenite. This content can be determined taking into account the ratios of the integrated intensities of the individual Bragg reflections of both phases weighted by a proportionality factor, which can be calculated from basic principles. Details can be found in (Laine 1978). The volume fraction of ferrite/martensite and austenite can be determined by the following equations taking into account each available pair of (*hkl*) reflections and calculating the mean. Other phases (i.e. carbides) can reasonable be neglected. Since phase transformations in the observed alloy system are located below 100°C a temperature dependence of the proportionality factors was not considered. During residual stress measurement integrated intensities under different tilt angles (ψ-angles) were additionally taken into account when determining the martensite to austenite ratio.

$$V_\alpha = \frac{1}{\left[1 + \left(\frac{R_{\alpha(hkl)}}{R_{\gamma(hkl)}} \frac{I_{\gamma(hkl)}}{I_{\alpha(hkl)}}\right)\right]} \tag{1}$$

$$V_\gamma = 1 - V_\alpha. \tag{2}$$

V_α is a volume fraction ferrite/martensite, V_γ volume fraction austenite, $I_\alpha(hkl)$ integrated intensity of individual ferrite/martensite reflection, $I_\gamma(hkl)$ integrated intensity of individual austenite reflection, $R_\alpha(hkl)$ proportionality factor of

individual ferrite/martensite reflection, and $R_{\gamma}(hkl)$ is a proportionality factor of individual austenite reflection.

Temperature Acquisition

Temperature acquisition during welding is complex due to the presence of the welding arc. In the present case the temperature distribution was obtained ex situ by means of thermal imaging, supported by thermocouples, using identical experimental conditions. Thermal imaging offers the advantage of fast two-dimensional temperature mappings. Neglecting a temperature gradient in the thin samples across the thickness, the measured temperatures can be directly assigned to the measured diffraction information. Table 4 gives details of the thermal imaging system.

Residual Stress Measurement

In order to determine the effect of the phase transformation temperature on the residual stress condition, phase-specific residual stress measurement was conducted in transmission geometry ex situ after welding. Altogether nine measuring points with a distance of 0.5 mm were selected in the weld with increasing depth beginning 1 mm under the weld surface ending at 5 mm. The residual stresses were determined for the martensitic and also the austenitic phase of the LTT weld. In addition equivalent measurements were made in a re-melted high-strength steel S690Q. Specimen size and welding parameters were identical. The measuring and evaluation parameters are shown in Table 5.

Table 4 Parameters of thermal imaging system

Optical resolution	640 × 480 infrared pixel (300 μm)
Temperature range	−40°C to >2000°C
Thermal resolution	1.5 K (0–100°C)/2% (>100°C)
Test frequency	5 Hz
Objective	50 mm

Table 5 Measurement and evaluation parameters of the residual stress measurements

Primary beam cross section	1 × 1 mm^2
Secondary aperture	Double slit system (equatorial × axial) 0.12 mm × 5 mm
Diffraction angle	$2\Theta = 6°$
Measuring mode	Transmission
Measuring time	100 s/spectrum
Evaluated diffraction lines	Ferrite/martensite: 110, 200, 211, 220; austenite: 111, 200, 220, 311
Calibration	Tungsten powder

The residual stresses were determined using the $\sin^2 \psi$ technique (Macherauch and Müller 1961). For that purpose the specimen was tilted 90° around the primary beam axis from $\psi = 0$ (specimen position as in Fig. 3) to $\psi = 90°$. Neglecting the presence of shear stresses in the material volume, the following equation is valid:

$$\frac{D_{\varphi=0,\psi} - D_0}{D_0} = \frac{1}{2} s_2^{\alpha',\gamma,\{hkl\}} \cdot \left(\sigma_{11}^{\alpha',\gamma} - \sigma_{33}^{\alpha',\gamma}\right) \cdot \sin^2 \psi + s_1^{\alpha',\gamma,\{hkl\}} \cdot \left(\sigma_{11}^{\alpha',\gamma} + \sigma_{22}^{\alpha',\gamma} + \sigma_{33}^{\alpha',\gamma}\right) + \frac{1}{2} s_2^{\alpha',\gamma,\{hkl\}} \sigma_{33}^{\alpha',\gamma}. \quad (3)$$

The lattice spacing $D_{\varphi=0,\psi}$ is a linear function of $\sin^2 \psi$. The slope of the plot $D_{\varphi=0,\psi}$ vs. $\sin^2 \psi$ can be solved for the term $\sigma_{11}^{\alpha',\gamma} - \sigma_{33}^{\alpha',\gamma}$. For the strain-free lattice spacing D_0 an approximation is sufficient. For this reason the phase-specific residual stresses shown in the following consist of a stress component $\sigma_{11}^{\alpha',\gamma}$ in longitudinal (welding) direction and a component $\sigma_{33}^{\alpha',\gamma}$ in normal (depth) direction. However, in the particular case $\sigma_{33}^{\alpha',\gamma}$ can be neglected, since in this direction an almost free shrinkage of the weld was present.

4 Results

Phase Transformation

In situ phase observation during welding is represented exemplarily in Figs. 6 and 7 by energy dispersive diffraction spectra (so-called density plots) as a function of time for the investigated materials in a distance of 1 mm to the weld surface. Additionally the d-spacing, what can easily be calculated from Bragg's law, is shown for selected Energies. Austenite to martensite phase transformations become clearly detectable on the basis of characteristic diffraction lines (indicated by white color in the plot) and can finally be assigned to the corresponding temperatures determined ex situ. Clearly, the phase transformation of the LTT weld can be identified in Fig. 6. The transformation is characterized by appearance of the 110α, 200α and 211α diffraction lines. In comparison Fig. 7 reveals that the phase transformation in case of cooling of the low alloyed, ferritic steel S690Q appears earlier and is therefore shifted to higher temperatures above 400°C according to the chemical composition. Due to the presence of δ-ferrite and the limited time resolution the transformation at this temperature is only indicated by disappearing of the 200γ and 311γ diffraction lines of austenite.

Determination of the phase contents during cooling of the LTT weld 1 mm below the surface shows that most of the transformation takes place during an interval of approximately 150 s between 71 and 52°C. After that the transformation decays. However, M_f is not reached, since retained austenite up to 50% is still present at ambient temperature, see Fig. 8. For reasons of microstructure (texture) the error represents up to ±43%.

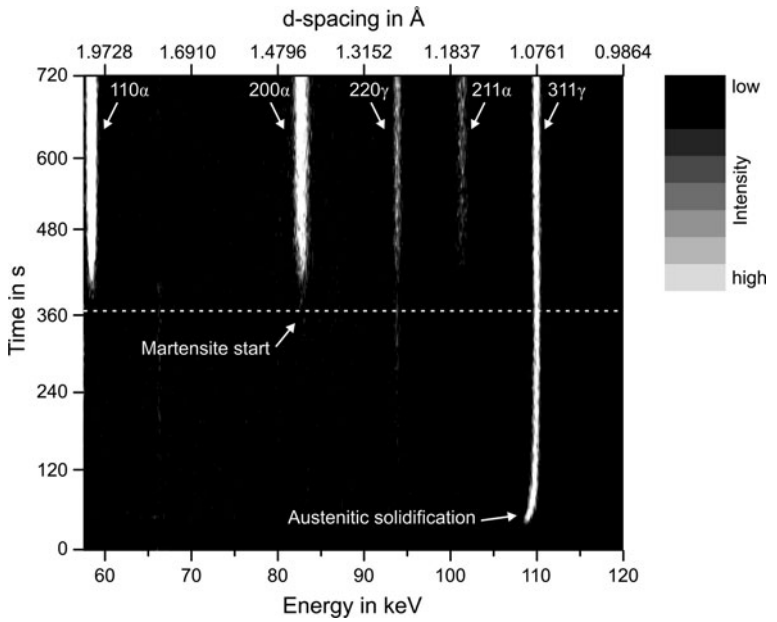

Fig. 6 2D density plot during cooling of the LTT weld showing primary austenitic solidification and transformation into martensite (1 mm below surface)

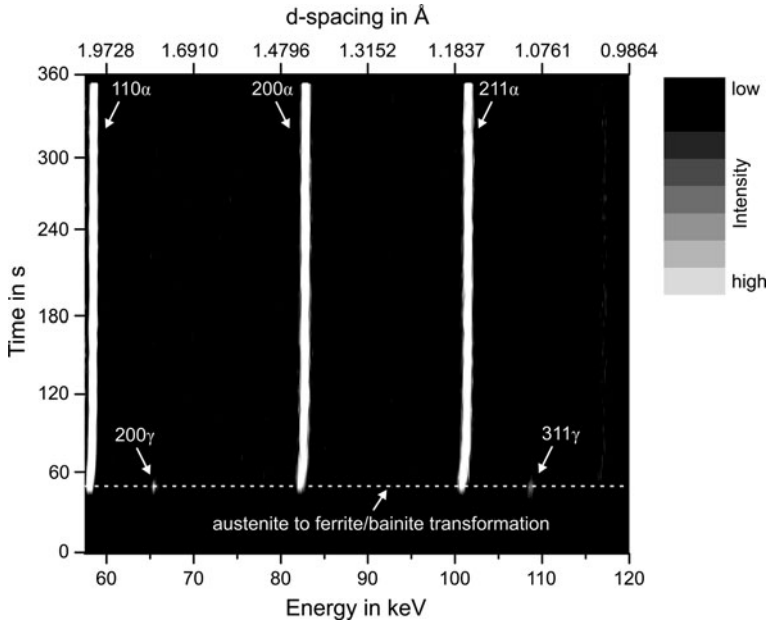

Fig. 7 2D density plot of ferritic steel S690Q indicating transformation into ferrite/bainite (1 mm below surface)

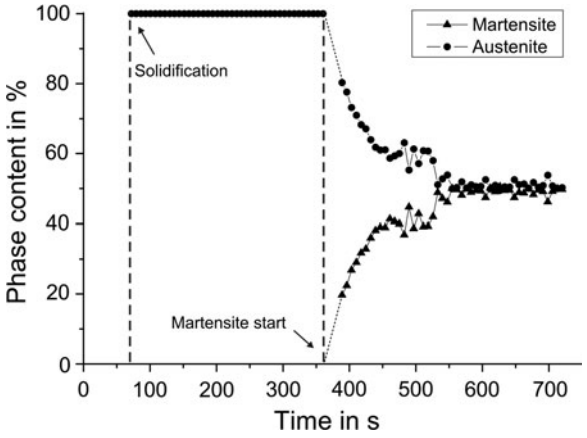

Fig. 8 Phase contents during cooling of the weld

With decreasing distance to the base material an increasing dilution and in particular reduction of nickel and chromium contents arises in the LTT weld. Therefore the transformation temperatures increase with approaching the base material. The relation of the chemical compositions determined by means of electron-beam micro probe analysis (shown as totally sum of the alloying elements Cr, Ni, C, Si and Mn) and the observed M_s-temperatures is represented in Fig. 9. In the following should be clarified how this temperature gradient influences the local residual stress distribution.

Residual Stresses

A comparison of the phase-specific residual stresses of the martensitic phase of the LTT weld as well as of the steel S690Q is shown Fig. 10. In the LTT weld high

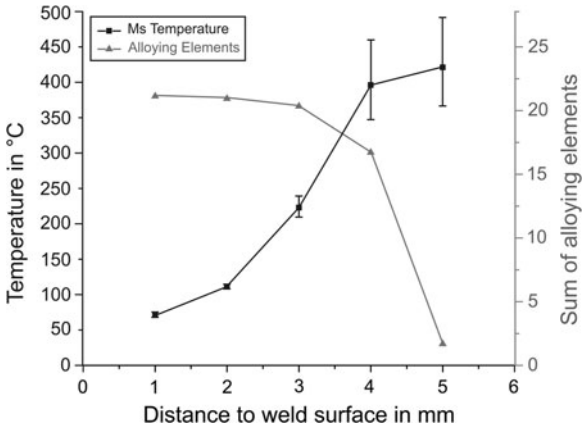

Fig. 9 M_s-temperature gradient caused by dilution compared to total sum of alloying elements, measured at varying distance to the weld surface

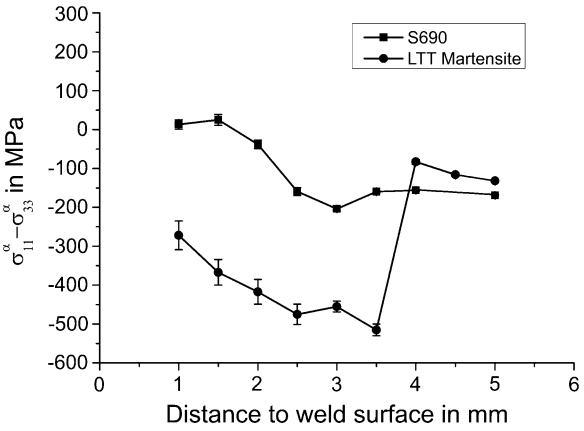

Fig. 10 Comparison of phase-specific residual stresses in the martensite of the LTT weld and S690Q

compressive residual stresses of up to −500 MPa are present. It is remarkable that with increasing distance to the weld surface the compressive residual stresses increase, although the M_s temperatures decrease (see Fig. 9). That can be ascribed to the M_s temperature gradient across the weld. Areas near the surface (low M_s) are influenced by shrinkage of already transformed areas far away from the surface (high M_s). Adjacent to the heat affected zone (4 mm)—according to the chemical compositions and transformation temperatures (see Fig. 9)—the stresses abruptly drop by 450 MPa to lower values.

Residual stresses in the ferritic steel S690Q initially show a qualitatively similar stress distribution, of increasing compressive stresses with increasing distance to the weld surface. The residual stresses exhibit lower values compared to the LTT weld at all, however without a stress decrease approaching the heat affected zone. This can be explained by the more or less constant chemical composition and therefore transformation temperatures above 400°C across the weld (small dilution effects).

The phase-specific residual stresses of the austenitic phase of the LTT alloy are shown in Fig. 11. In comparison to the martensitic phase the stress values are

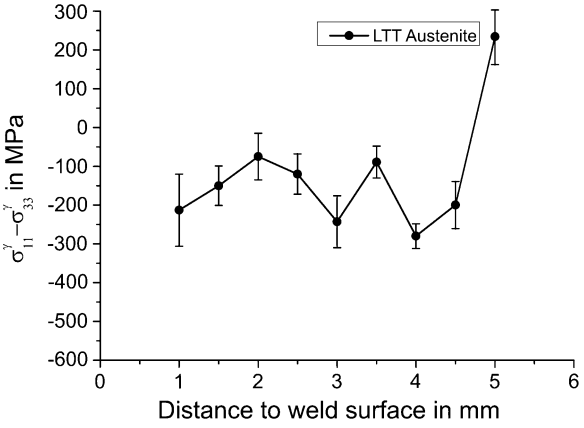

Fig. 11 Phase-specific residual stresses in austenite

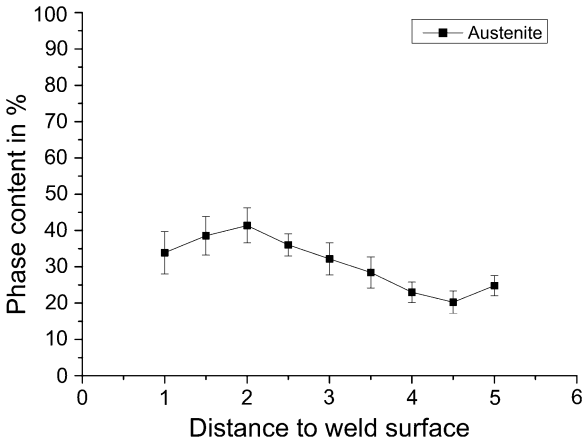

Fig. 12 Content of retained austenite dependent on the distance to the weld surface

lower. However, the stresses are also compressive up to −250 MPa. The retained austenite content in the LTT weld varies between 20 and 45% (see Fig. 12). Lower austenite contents are existent adjacent to the heat affected zone, caused by the high dilution here. However, a clear correlation between the content of retained austenite and the height of the phase-specific residual stresses cannot be found. Shortly before the transition to the heat affected zone (5 mm) the stresses of the austenitic phase also drop approximately by 450 MPa, as observed in the martensite.

Finally, the in-service-behavior of a joint is determined by the macro stresses. These can be calculated by means of a simple lever rule considering the phase-specific residual stresses and content of the individual phases (see Eq. 4).

$$\sum_{\alpha=1}^{n} p^{\alpha}\sigma^{\alpha} = \sigma^{M}. \tag{4}$$

α is a phase, p^{α} phase content, n number of phases, σ^{α} phase-specific residual stress, and σ^{M} is a macro residual stress.

The macro residual stresses of the LTT alloy compared to residual stresses of the ferritic/bainitic phase of the steel S690Q are shown in Fig. 13. The stresses of the LTT weld show a parallel shift to lower values caused by the lower stress level of the austenite. However, it remains a large difference compared to S690Q of up to 300 MPa. Furthermore, adjacent to the heat affected a stress drop by 300 MPa to the stress level of S690Q remains also.

5 Summary

High-energy polychromatic synchrotron radiation was used for the first time for in situ diffraction analysis of transformation kinetics during a real welding process

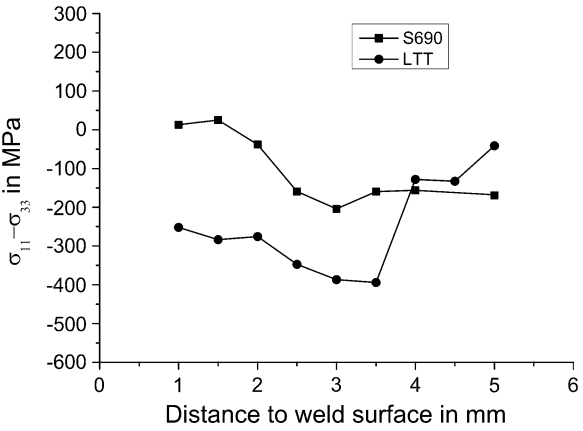

Fig. 13 Comparison of macro residual stresses in LTT weld and S690Q

and the determination of the resulting residual stresses. Spatial and time-resolved diffraction measurements were carried out investigating novel low transformation temperature alloys, which exhibit a γ–α'-phase transformation at comparatively low temperatures. The transformation behavior during welding could be determined in situ by means of energy dispersive diffraction analyses on the basis of characteristic diffraction lines. Finally, the resulting phase-specific residual stresses of martensite and austenite could be determined in the weld. Considering the content of each phase, it could be demonstrated that high compressive residual stresses up to -400 MPa can be reached according to lowered M_s temperatures. Future work shall clarify, how M_s temperature and varying amounts of retained austenite influence the level and distribution of residual stresses in the weld and adjacent areas. Further, it remains to be clarified how the observed compressive residual stresses are transferable to welded joints exhibiting shrinkage restraint.

Acknowledgements This research project is promoted by the DFG (German Research Foundation) (GI 376/2 1 and RH 1648/2 1). The authors would like to acknowledge the team of the EDDI beam-line of the Helmholtz Association for their kind support and Lincoln Electric Europe for provision of the LTT alloy.

References

Alexandrov BT, Lippold JC (2004) Methodology for in situ investigation of phase transformations in welded joints. IIW-Doc., IX-2114-04, pp 1–13

Babu SS, Elmer JW, Vitek JM, David SA (2002) Time-resolved X-ray diffraction in Fe-C-Al-Mn steel welds. Acta Mater 50:4763–4781

Bhadeshia HKDH (2004) Developments in martensitic and bainitic steels: role of the shape deformation. Mater Sci Eng A A378:34–39

Dai H, Francis JA, Stone HJ, Bhadeshia HKDH, Withers PJ (2008) Characterizing phase transformations and their effect on ferritic weld residual stresses with X-rays and neutrons. Metall Mater Trans A 39A:3070–3078

Eckerlid J, Nilsson T, Karlsson L (2003) Fatigue properties of longitudinal attachments welded using low transformation temperature filler. Sci Technol Weld Join 8(5):353–359

Elmer JW, Wong J, Ressler Th (2000) Observations of phase transformations during solidification and cooling of austenitic stainless steel welds using time-resolved X-ray diffraction. Scr Mater 43:751–755

Genzel Ch, Denks IA, Gibmeier J, Klaus M, Wagener G (2007) The materials science synchrotron beamline EDDI for energy-dispersive diffraction analysis. Nucl Instrum Methods Phys Res A 578:23–33

Kannengiesser Th, Kromm A, Rethmeier M, Gibmeier J, Genzel C (2008) Residual stresses and in situ measurement of phase transformation in low transformation temperature (LTT) welding materials. Adv X-ray Anal 52:755–762. ISSN 1097-0002

Kromm A, Kannengiesser Th (2009) In situ-phase analysis using synchrotron radiation of low transformation temperature (LTT) welding material. Soldagem Insp São Paulo 14(1):82–88

Kromm A, Kannengiesser T, Gibmeier J, van der Mee V (2009) Determination of residual stresses in low transformation temperature (LTT-) weld metals using X-ray and high energy synchrotron radiation. Weld World 53:3–16

Laine E (1978) A high-speed determination of the volume fraction of ferrite in austenitic stainless steel by EDXRD. J Phys F Met Phys 8(7):1343–1348

Macherauch E, Müller P (1961) Das $\sin^2\psi$-Verfahren der röntgenographischen Spannungsmessung. Z Angew Physik 13(7):305–312

Ohta A, Watanabe O, Matsuoka K, Shiga C, Nishijima S, Maeda Y, Suzuki N, Kubo T (1999) Fatigue strength improvement by using newly developed low transformation temperature welding material. Weld World 43(6):38–42

Spiess L, Teichert G, Schwarzer R, Behnken H, Genzel C (2009) Moderne Röntgenbeugung Röntgendiffraktometrie für Materialwissenschaftler. Physiker und Chemiker, Wiesbaden: Vieweg Teubner. ISBN: 978-3-8351-0166-1

Terasaki H, Komizo Y, Yonemuira M, Osuki T (2006) Time-resolved analysis of phase evolution for the directional solidification of carbon steel weld metal. Metall Mater Trans A 37A:1261–1266

Wang W, Huo L, Zhang Y, Wang D, Jing H (2002) New developed welding electrode for improving the fatigue strength of welded joints. J Mater Sci Technol 18(6):527–531

http://www.springer.com/978-3-642-14793-7

In-situ Studies with Photons, Neutrons and Electrons Scattering

Kannengiesser, Th.; Babu, S.S.; Komizo, Y.-i.; Ramirez, A. (Eds.)

2010, XII, 204 p., Hardcover
ISBN: 978-3-642-14793-7